NASCAP-2K SIMULATIONS OF A VLF PLASMA ANTENNA

M. J. Mandell, (858) 826-1622, Myron.J.Mandell@saic.com
V.A. Davis, (858) 826-1608, Victoria.A.Davis@saic.com
Science Applications International Corporation
10260 Campus Point Dr., M.S. A1
San Diego, CA, 92121 (FAX: 858-826-6584)

D. L. Cooke, A.T. Wheelock
Air Force Research Laboratory, Space Vehicles Directorate
Hanscom Air Force Base, MA 01731 (FAX: 781-377-2491)

Christopher J. Roth
Radex Inc.
131 Hartwell Ave. Lexington MA, 02421-3126

Abstract

The response of a plasma to very low frequency (VLF) (3 kHz to 20 kHz) antennas at orbital altitudes of 1000 to 10,000 kilometers has been a subject of scientific interest for many decades.[1,2,3] As this antenna frequency is less than either the plasma frequency or the electron gyrofrequency (both nearly 300 kHz for a plasma density of 10^9 m^{-3} and a magnetic field of 0.1 gauss), only certain modes can propagate as an electromagnetic (EM) wave, and the near field is dominated by electrostatic (ES) effects. Although a comprehensive self-consistent EM-ES simulation would be the desired goal, there are many computational challenges to be overcome, so we begin with a quasi-static simulation so as to sort out the dominant ES effects.

We present antenna simulations using *Nascap-2k* modeling the plasma using both an explicit Particle-in-cell (PIC) approach and a hybrid approach with PIC ions and fluid barometric electron densities. In the latter, electron plasma oscillations are suppressed, while in the former they are excited. Accuracy of the simulations is assessed by comparison with lower-dimensional simulations of similar cases.

Introduction

Observations of electron precipitation attributed to Very Low Frequency (VLF) (~20 kHz) transmissions of human origin were published[1,2,3,4] during the 1970s and 1980s. Such precipitation is thought to be a major lifetime-limiting factor for energetic radiation belt electrons.[5,6] There is current interest in generating VLF waves in space to perform controlled experiments to study the interaction of VLF waves with these electrons.[7] A transmitting antenna for this purpose would be several inches in diameter and at least several meters long, and have bias amplitudes of at least several hundred volts. Previous studies have demonstrated that the antenna impedance is substantially affected by the space plasma.[8,9] In addition, by interacting with a large volume of the surrounding plasma, the antenna could have a major effect on spacecraft potential. Thus, it is of major interest to be able to simulate the antenna dynamically and in three dimensions together with its host spacecraft and the surrounding plasma.

Nascap-2k (NASA Air Force Spacecraft Charging Analyzer Program 2000) is a modern spacecraft charging code, replacing the older codes NASCAP/GEO, [10,11,12] NASCAP/LEO, [13,14] POLAR, [15] and DynaPAC. [16,17,18,19] *Nascap-2k* implements all capabilities and algorithms from DynaPAC, allowing the user to perform dynamic plasma response simulations. Specifically, *Nascap-2k* incorporates the Particle-in-Cell (PIC) features needed to do this type of problem. In studying the CHAWS experiment (Charging Hazards and Wake Studies[20]), ion trajectories were used to calculate steady-state, self-consistent charge densities and space potentials. In *Nascap-2k*, we have developed the ability to do Hybrid-PIC, *i.e.*, PIC ions with barometric (or Boltzmann) electron densities. For the antenna problem, we would like to follow both electrons and ions using PIC. It is important to note, however, that *Nascap-2k* currently only solves Poisson's equation, rather than the full Maxwell equations, so it computes only curl-free, quasi-static fields. Near-term development plans include electro-dynamic improvements to *Nascap-2k*.

In this paper, we describe the antenna problem and, for baseline parameters, show the solution as calculated by a 1-D PIC code for electron dynamics in the sheath. We then pose a nearly identical problem for solution with *Nascap-2k*, demonstrate that the solutions agree, and show the graphics. We also use the Hybrid-PIC capability to study the ion dynamics for several wave cycles at frequencies above and below the ion plasma frequency.

Statement of Problem

The objective of these initial calculations is to simulate the dynamic sheath around a negative thin rod. We avoid positive polarity because the positive half of the antenna collects copious electrons, so the maximum potential it can reach is determined by numerous unknown factors, such as the relative size of the spacecraft and antenna, but for any reasonable parameters is limited to a very few volts positive. We wish to do this with realistic values of plasma density, ion mass, applied voltage and frequency, magnetic field, and spacecraft velocity. The arbitrary directions of the latter two require a three-dimensional code. A one-dimensional (radial) code can handle magnetic field either parallel to the antenna or circumferential (as would be caused by current flowing in the antenna).

Sheath Size Estimate

The sheath (defined as the region from which electrons are excluded) can be quite large, even for a fairly modest potential of about 100 V. To estimate the sheath size, we specify the electric field at the antenna radius, R_0. We assume that the external space between the antenna and the sheath is filled with ions at ambient density, ρ. The electric field at any radius, r, between the antenna and the sheath is

$$E(r) = \frac{\rho e(r^2 - R_0^2)}{2\varepsilon_0 r} - \frac{R_0}{r} E(R_0)$$

The sheath condition is $E(R_s)=0$, where R_s is the sheath radius. We then integrate the electric field from R_s to R_0 to determine the corresponding potential. Figure 1 shows the relation between applied potential and sheath radius for a 10 cm diameter antenna. At a density of 10^{12} m^{-3}, the sheath radius at 100 V bias is about 15 cm, and grows to nearly a meter at a density of 10^{10} m^{-3}. The one-dimensional and three-dimensional full PIC calculations that follow assume a density of 3×10^{11} m^{-3}, giving a sheath radius of about 20 cm. The hybrid PIC calculations were performed for a 20 cm diameter antenna in a plasma with density 1×10^{10} m^{-3}, giving a sheath radius of about 80 cm.

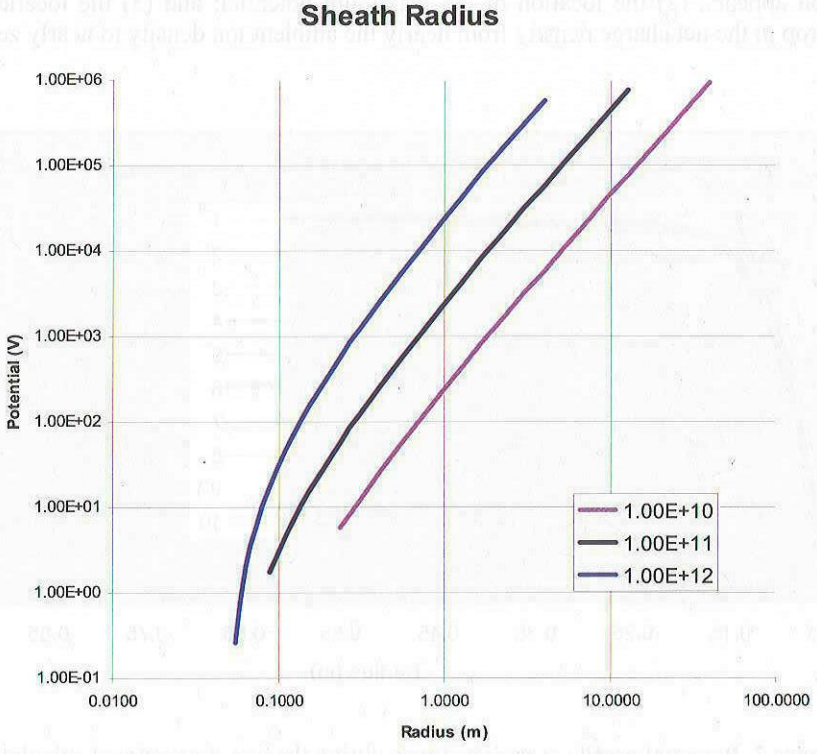

Figure 1. Potential versus sheath radius for negative applied potential on a 10 cm diameter antenna. Curves for three different plasma densities are shown.

Baseline Parameters for Full PIC Calculations

Table 1 shows the baseline parameters for the calculation. A density of 3×10^{11} m^{-3} is chosen so that the sheath is large compared with the wire, but still very tractable computationally. In general the plasma is cold, so 0.1 eV is used in those places where temperature is required. The antenna frequency is set to 100 kHz, and the plasma response is followed for a half-period of 5 μs. To see the effect of magnetic field, a field of 0.5 gauss is chosen. The ordering of the plasma frequency, electron gyrofrequency, and applied frequency is $\omega_p > \omega_c > 2\pi f$.

Table 1. Parameters for baseline calculations.

Plasma Density	3×10^{11} m^{-3}
Electron Temperature	0.0 or 0.1 eV
Plasma Frequency	3.1×10^{7} s^{-1}
Antenna Frequency	100 kHz
Magnetic Field	0.0 or 0.5 gauss
Electron Gyrofrequency	0.0 or 8.8×10^{6} s^{-1}
Ion Species	O^{+}

One-dimensional Calculations

A simple one-dimensional finite element code was written to simulate quasistatic plasmadynamics about a long cylindrical antenna. The computational domain extended out to one meter from an antenna radius of 5 cm and was divided into 1000 zones in equal increments of r^2. Two ion macro-particles and two electron macro-particles were placed in each zone, with each macro-particle having equal charge. The simulation was run for 2000 timesteps of 2.5 ns each, making up the 5 μs half-period for the 100 kHz frequency. When electrons left the computational space they were replaced as thermal electrons at the boundary.

Figure 2 shows the potential profile at various times in the calculation. As expected, the potential is rapidly screened to about the expected sheath radius as electrons are expelled from the sheath. At certain times a positive potential region appears. This is an effect of electron inertia, as the moving electrons do not stop of their own accord, but must be attracted back toward the sheath boundary. In Figure 3 through Figure 5 we plot (1) the maximum potential at times when a positive region appears; (2) the location of the maximum potential; and (3) the location of the sheath edge, indicated by a sharp drop in the net charge density from nearly the ambient ion density to nearly zero.

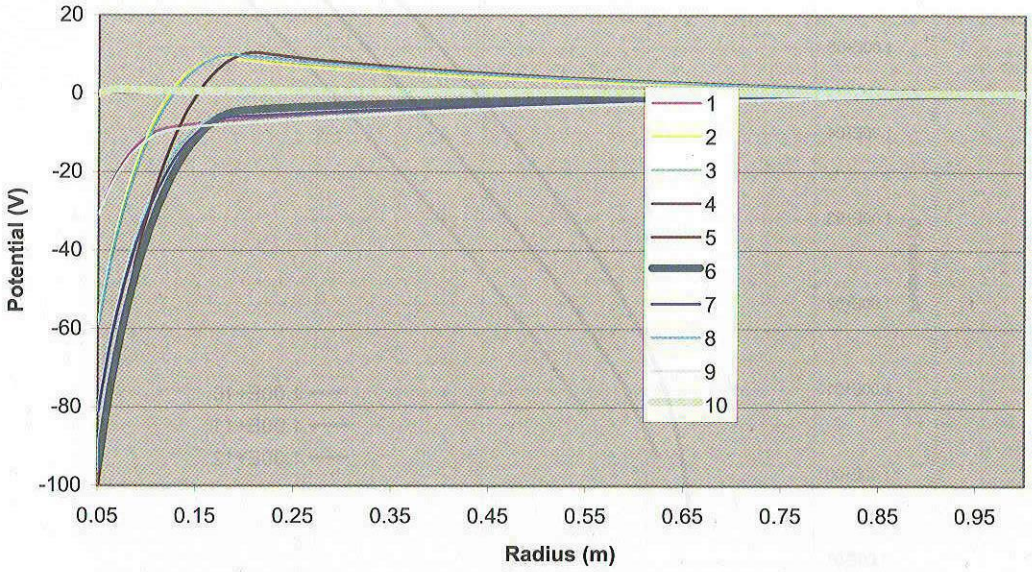

Figure 2. Potential profile at various times during the one-dimensional calculation.

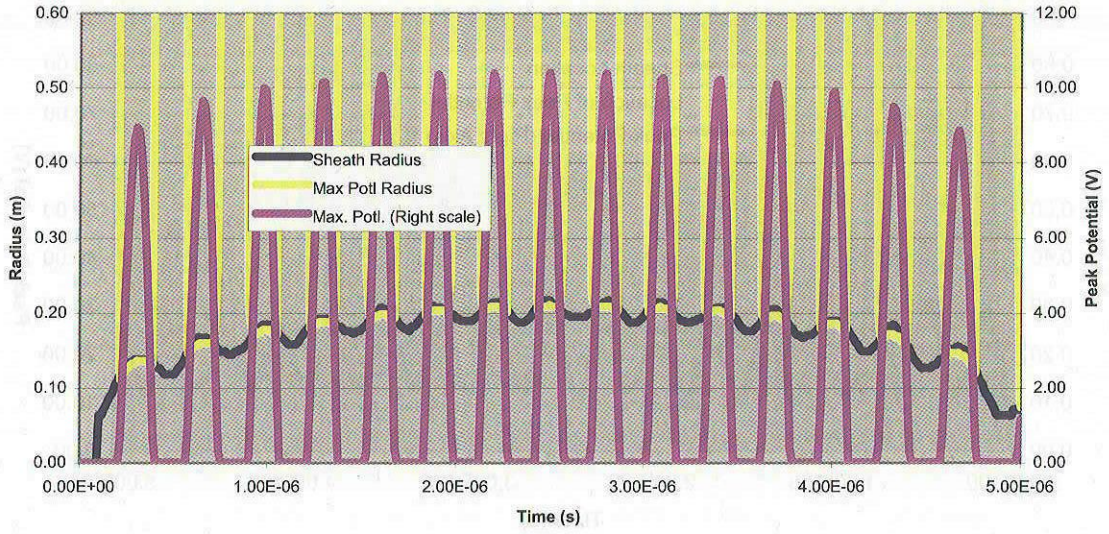

Figure 3. Simulation results for half sine wave and no magnetic field, showing peak positive potential (magenta curve, right scale), location of peak (yellow curve, left scale) and location of sheath edge (dark curve, left scale).

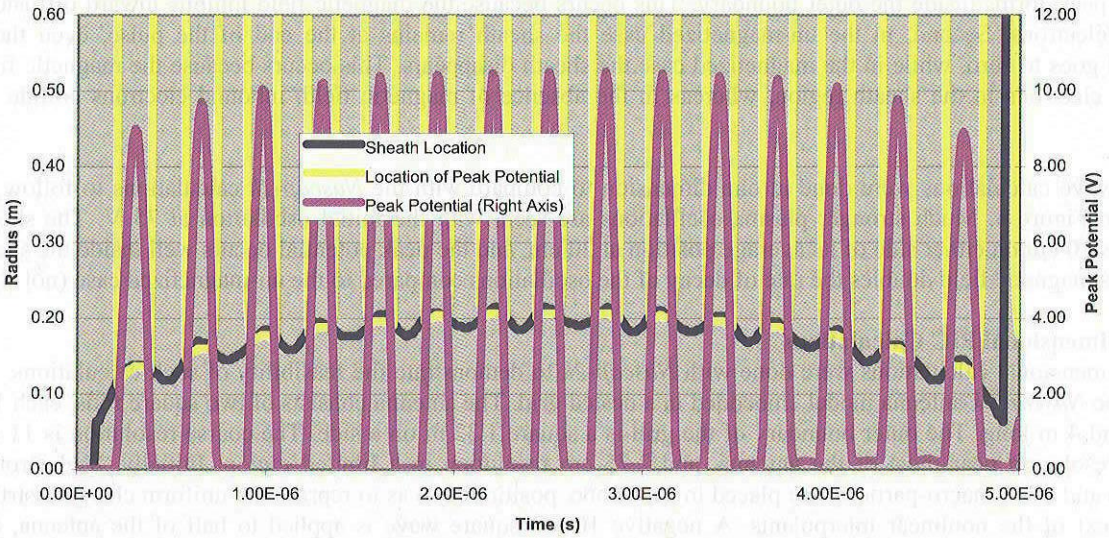

Figure 4. Same as Figure 3, for half sine wave with magnetic field of 0.5 gauss.

Figure 3 and Figure 4 show results for a half sine wave, for which the applied negative potential continuously rises and returns to zero. The magnitude of the potential maximum is 8 to 10 V, and the oscillation frequency is somewhat less than the electron plasma frequency. The sheath edge occurs at a radius of about 20 cm as calculated above, with oscillations of about two cm. The potential maximum, when it occurs, is just inside the sheath edge.

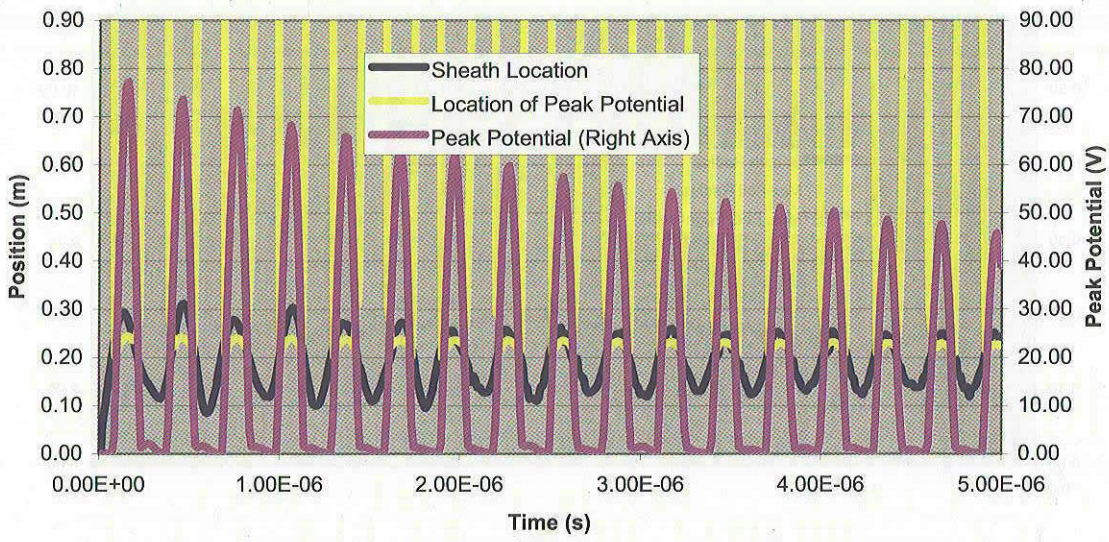

Figure 5. Same as Figure 3, for square wave with 0.5 gauss magnetic field.

Two differences can be noted between the un-magnetized (Figure 3) and magnetized (Figures 4 and 5) cases. First, in the un-magnetized case the potential goes completely non-positive between peaks, whereas in the magnetized case a positive peak forms inside the outer boundary. This occurs because the magnetic field inhibits inward diffusion of the thermal electrons. Second, in the un-magnetized case the sheath remains at the end of the pulse, even though the potential goes to zero, while in the magnetized case the sheath disappears. This occurs because the magnetic field traps inbound electrons in the sheath region, whereas in the absence of magnetic field, inbound electrons collide with the antenna.

Square wave calculations were done in one dimension to compare with the *Nascap-2k* calculations to follow, and are shown in Figure 5. Much stronger plasma oscillations are seen, with the initial oscillation at 75 V. The sheath edge oscillates 10 cm on either side of its average position at 20 cm, and the peak potential occurs well inside the sheath. The 0.5 gauss magnetic field doubles the rate of decay of the oscillations compared to the un-magnetized case (not shown).

Three-dimensional PIC Calculations

Three-dimensional calculations were done with *Nascap-2k* to demonstrate the feasibility of such calculations. Figure 6 shows the *Nascap-2k* antenna model embedded in a nested grid. The antenna consists of two square rods, each 10 cm on a side and 4 m long. The outer boundary of the grid is a square 1.32 m on a side. The coarse resolution is 11 cm, with 5.5 cm resolution near most of the antenna, and 2.75 cm resolution in a limited region. Initially, 8 electron macro-particles and 8 ion macro-particles are placed in each zone, positioned so as to represent a uniform charge distribution in the context of the nonlinear interpolants. A negative 100 V square wave is applied to half of the antenna, and each timestep consists of (1) tracking the particles for 2.5 ns, (2) sharing the particle charge to the nodal coefficients in accordance with the nonlinear interpolants, and (3) recalculating the potential in preparation for the next tracking phase.

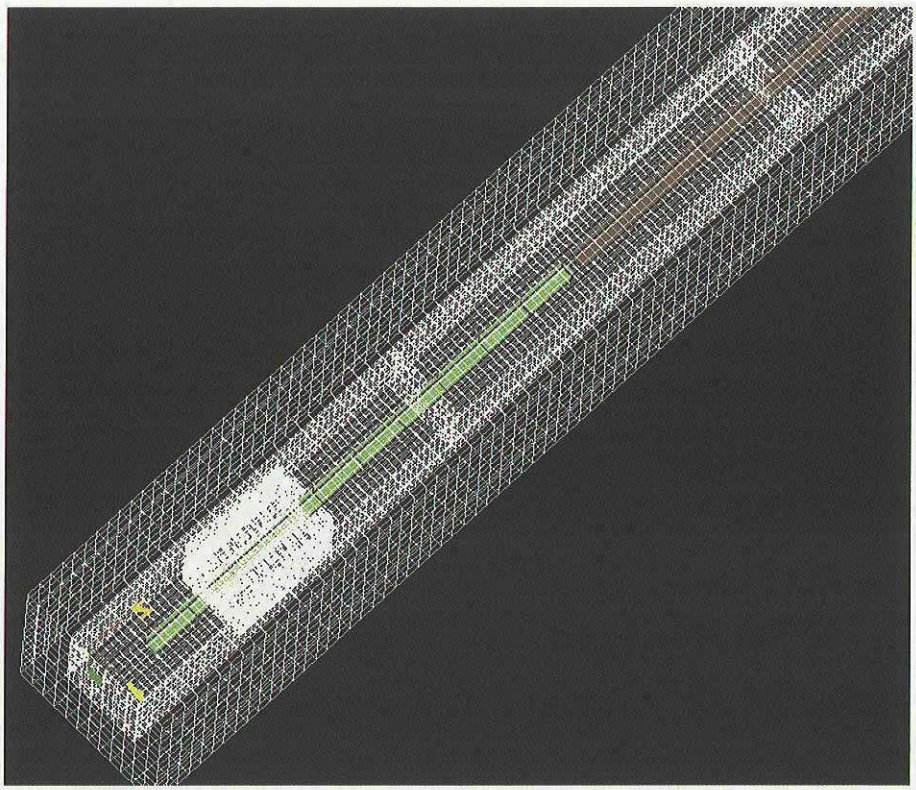

Figure 6. *Nascap-2k* antenna model, showing antenna and gridding.

The initial state is represented in a three-dimensional view in Figure 7 and a planar view in Figure 8. These figures show the potential in a cut plane, and a plane of nearby electron macro-particles. The ion macro-particles have the same initial configuration, but move negligibly during the simulation time. Note that the apparent high density of particles in the subdivided region is balanced by correspondingly reduced particle weight. Figure 9 show close-ups of the simulation at later times. The left figure shows the electron motion at 50 ns leading to a sheath radius of 18 cm. Note the effects of the square cross-section. Particles that started out near the flat, low-field region have moved considerably less than those that started out near the high-field corners. Figure 9-right shows the configuration at time of maximum positive potential (137 ns). At this time, there is a high, broad maximum in the potential, with electrons excluded from a region that extends well beyond the location of the potential maximum.

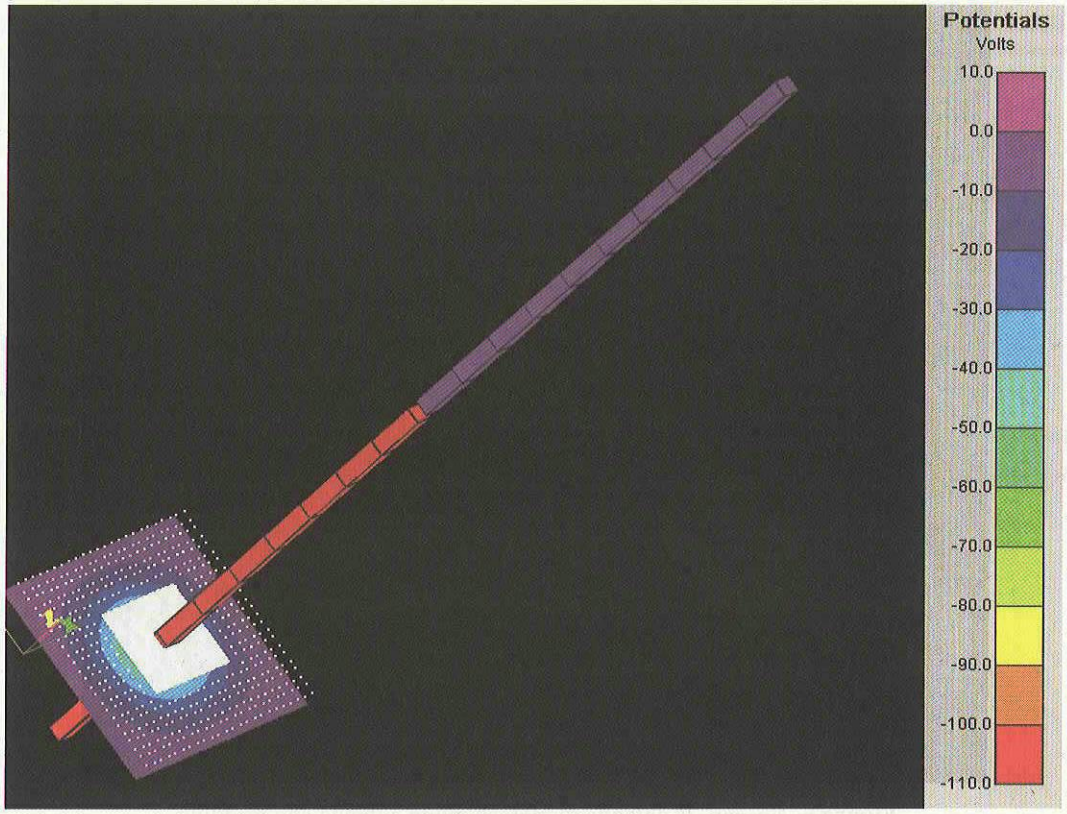

Figure 7. *Nascap-2k* antenna model showing potentials and particle positions after 2.5 ns.

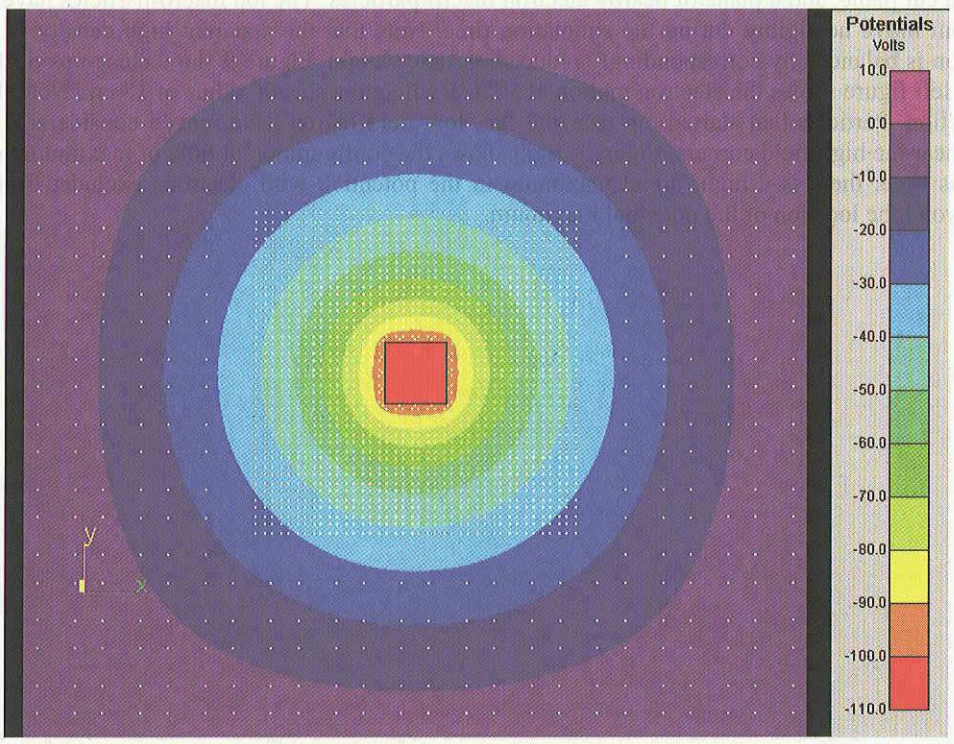

Figure 8. Planar view of initial potentials and particles, as shown in Figure 7.

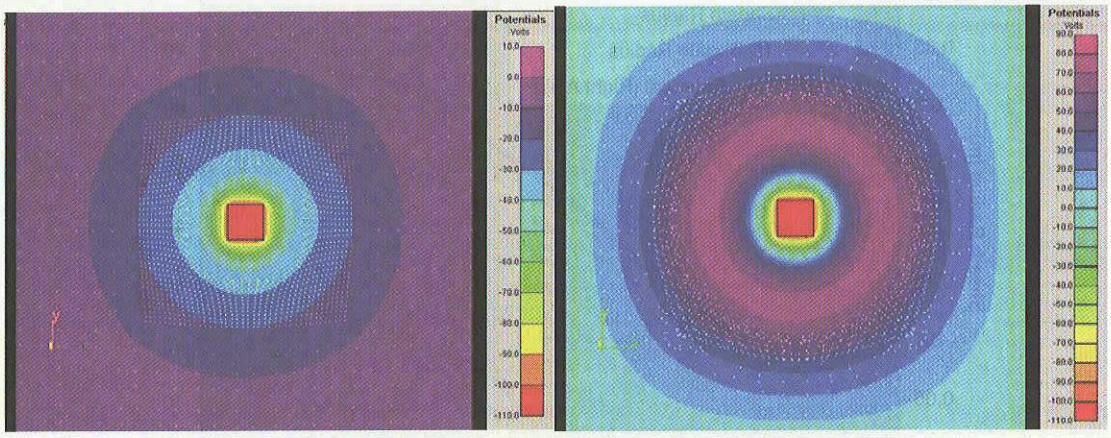

Figure 9. Blowups of electron macro-particles and potentials. Left: sheath radius of about 18 cm after 50 ns. Right: at time of maximum positive potential (137 ns).

Figure 10 shows another view of the final configuration, with potentials in a plane containing the antenna. Note that there is no apparent difference between the potentials in the highly resolved region and in the less resolved region, suggesting that the highest level of resolution may not be needed.

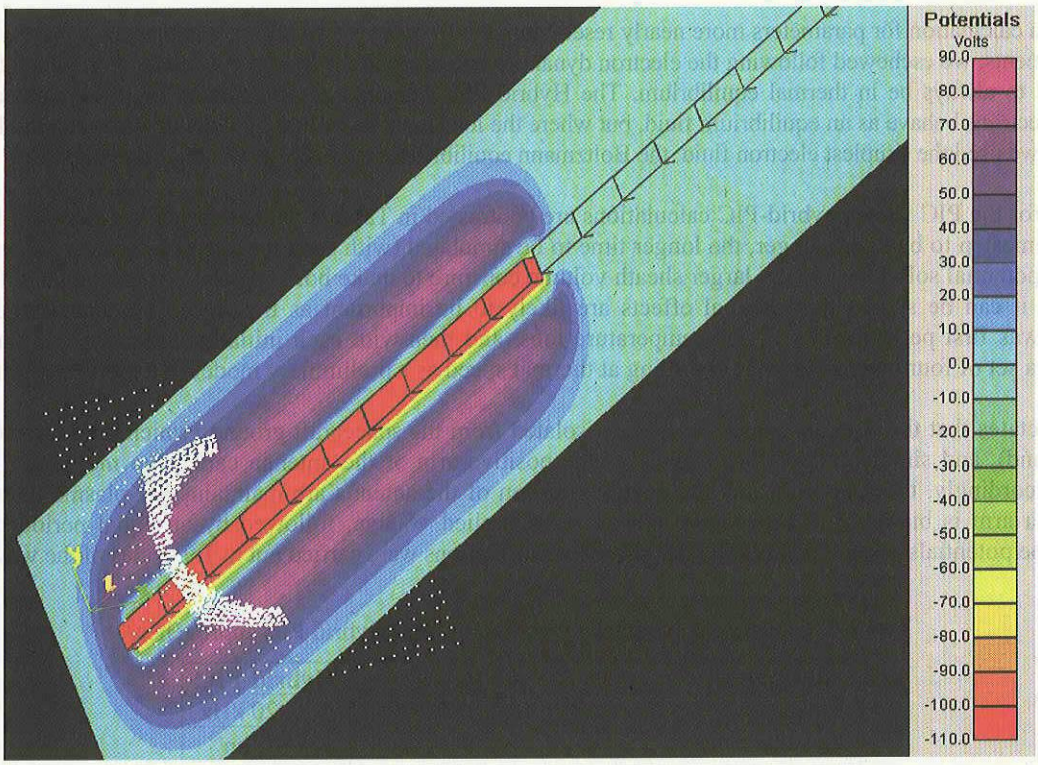

Figure 10. Another view of the final configuration (at 137.5 ns), showing potentials in a plane containing the antenna.

Figure 11 shows the development of the sheath radius and maximum potential calculated by *Nascap-2k*, compared with the one-dimensional sheath radius result. The maximum potential of 75 V, as well as the time of first maximum (140 ns) is in excellent agreement with the one dimensional result. The maximum sheath radius calculated by *Nascap-2k* is larger than the one-dimensional result in proportion to the effective larger size of the 10 cm square antenna vs. the 10 cm diameter round antenna.

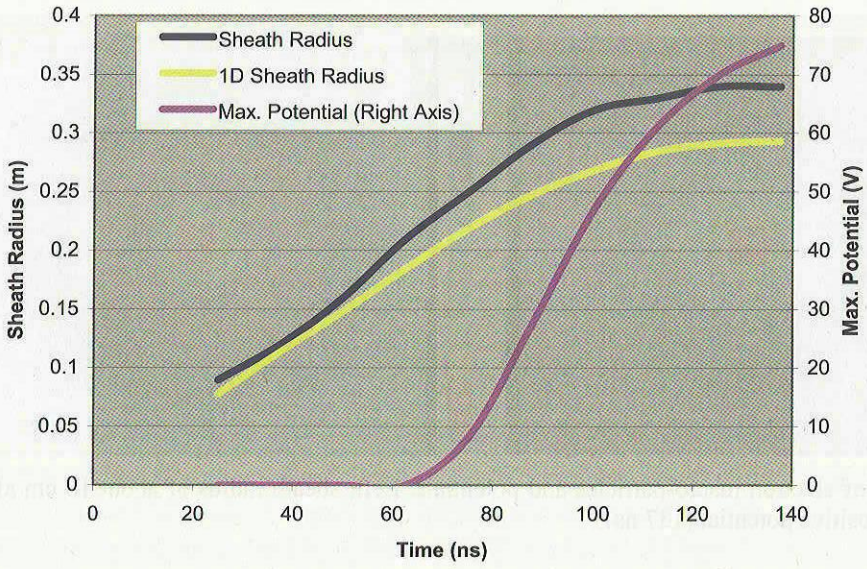

Figure 11. *Nascap-2k* results for sheath radius (dark curve) and maximum potential (magenta curve, right scale) compared with one-dimensional sheath radius results (yellow curve).

Hybrid-PIC Calculation

To perform a calculation for parameters more nearly resembling the frequency, waveform, and plasma density of interest for VLF experiments, we eschewed following the electron dynamics and adopted the hybrid-PIC method, in which the electrons are assumed to always be in thermal equilibrium. The Hybrid PIC technique is appropriate for low frequency problems where the electrons behave as an equilibrium fluid, but where the ions must be treated as a kinetic gas using the PIC method. In this case, we used the simplest electron fluid, the Boltzmann equilibrium, and only the O^+ ions were tracked.

Parameters for the PIC versus hybrid-PIC calculations are contrasted in Table 2. Note that while the hybrid-PIC method allows the timestep to be much longer, the longer time to be simulated (with each timestep requiring a particle push and a nonlinear potential solution) and the larger sheath volume conspire to make both calculations of comparable difficulty. In addition, it can be shown that thermal effects are likely to be important as the sheath becomes large. Thus, the calculation was first performed with zero-temperature ions, and then with each initially stationary ion macro-particle replaced by a set of four macro-particles diverging at thermal speed as a preliminary model of a thermal distribution.

Prudence dictates that the antenna center tap be DC-isolated from the spacecraft ground (which therefore remains near plasma ground), and simple calculations show that the positive arm of the antenna cannot go more than a few volts positive. Accordingly, the spacecraft and the positive portion of the antenna are maintained at plasma potential, while each antenna arm is biased with a negative half-cycle of applied voltage, followed by an equal period of near-zero potential. The potentials are solved at each time step. The calculations were carried out to 1.9 cycles of the wave.

Table 2. Contrasting parameters for the PIC and Hybrid PIC approaches.

Parameter	PIC	Hybrid-PIC
Frequency	100 kHz	2, 6, 20 kHz
Plasma Density	3×10^{11} m^{-3}	1×10^{10} m^{-3}
Plasma Frequency (electron)	4.92 MHz	898 kHz
Plasma Frequency (Oxygen)	28.5 kHz	5.2 kHz
Peak applied potential	-100 V	-100 V
Waveform	Square wave	Sine Wave
Sheath radius	34 cm	80 cm
Timestep	2.5 ns	1/50f
Time Simulated	0.140 μs	2/f
Antenna Length	4 m	10 m
Antenna Radius	0.05 m	0.1 m
Initial No. of Electrons (Ions)	350,000	966,000

A snapshot of the 2 kHz, zero temperature calculation is shown in Figure 12. The figure shows the potentials in a cut plane midway through the negative end of the antenna. Although only a representative subset of the ion macro-particles is shown, the figure still illustrates that *Nascap-2k* can perform these calculation with a relatively low number of particles compared to more common approaches to PIC. This is because *Nascap-2k* uses a high order finite element potential solver. The *Nascap-2k* potential solver uses non-linear interpolating functions that guarantee strictly continuous electric fields as well as potentials. This dramatically reduces the electric field noise that otherwise forces the calculation to use orders of magnitude more particles and accordingly more time. These simulations took on the order of 1 day on a dedicated GHz PC.

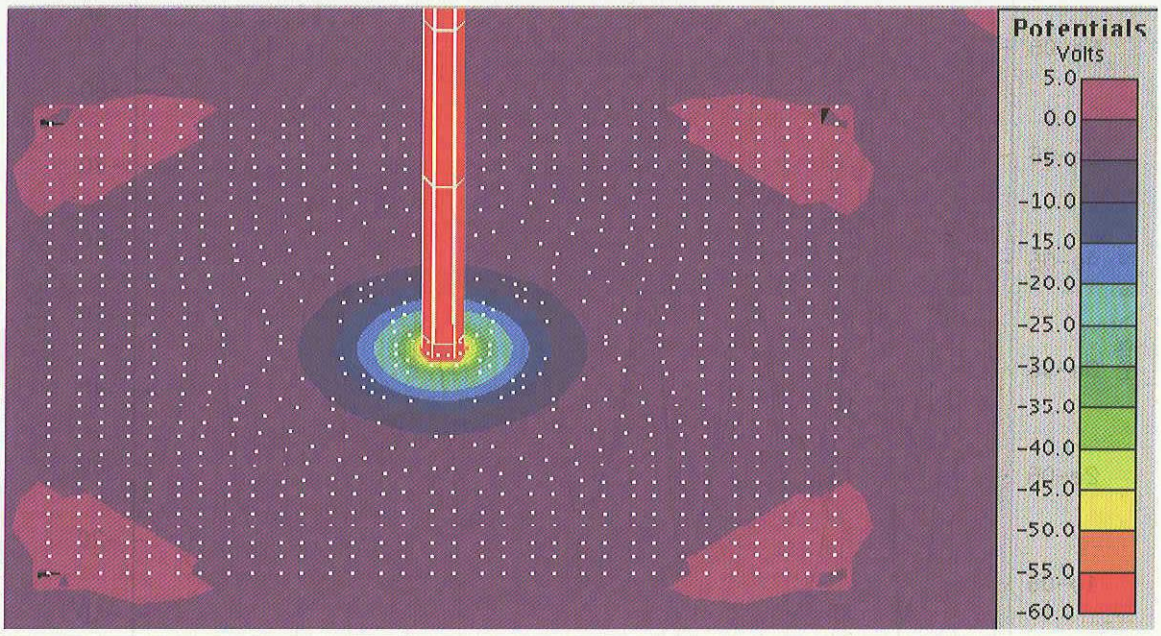

Figure 12. Subset of ion positions and potentials from 2 kHz model at time step 20 at an antenna voltage of –59 Volts.

The calculations do not reach a fully repeating state, but the cycle to cycle variations are small enough that we can draw some preliminary conclusions. Figure 13 shows a summary of the collected ion current for the three calculations at zero temperature and frequencies of 2, 6, and 20 kHz. The ion plasma frequency is 5 kHz. The current is in phase with the voltage for the 2 kHz case, but lags increasingly as the applied frequency exceeds the ion plasma frequency. For the 20 kHz case the collected current appears to develop harmonics close to the ion plasma frequency.

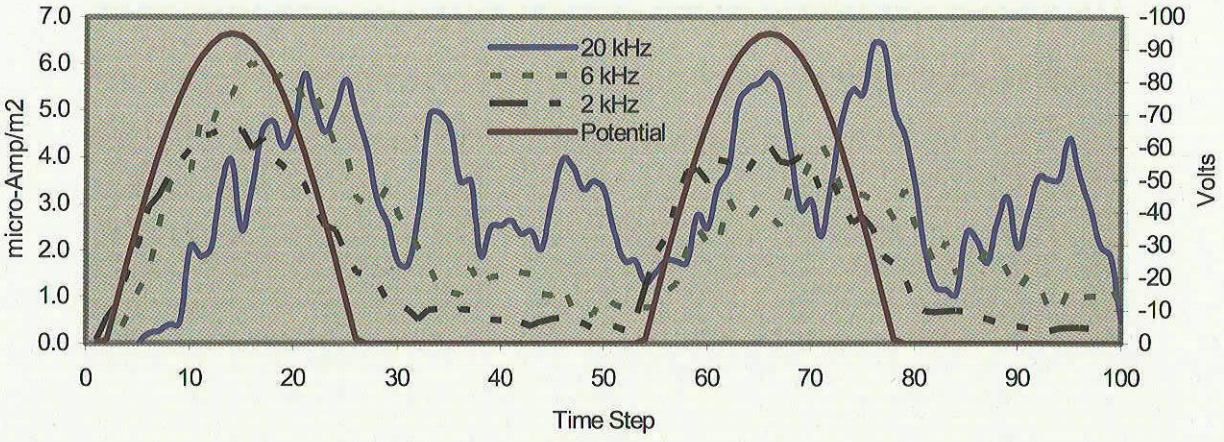

Figure 13. Current and voltage history for the Hybrid PIC calculations at zero temperature for three different frequencies.

We used a preliminary model of a finite temperature plasma in which each initial ion macro-particle is replaced with four macro-particles moving a thermal speeds in the plane normal to the antenna. The results are shown in Figures 14 through 16. For the 2 kHz and 6 kHz cases (Figure 15) the thermal distribution made no significant difference, other than to smooth the results. For the 20 kHz case (Figure 16) we were able to run 6 cycles, with the latter three showing a smooth, steady-state, albeit anharmonic current waveform.

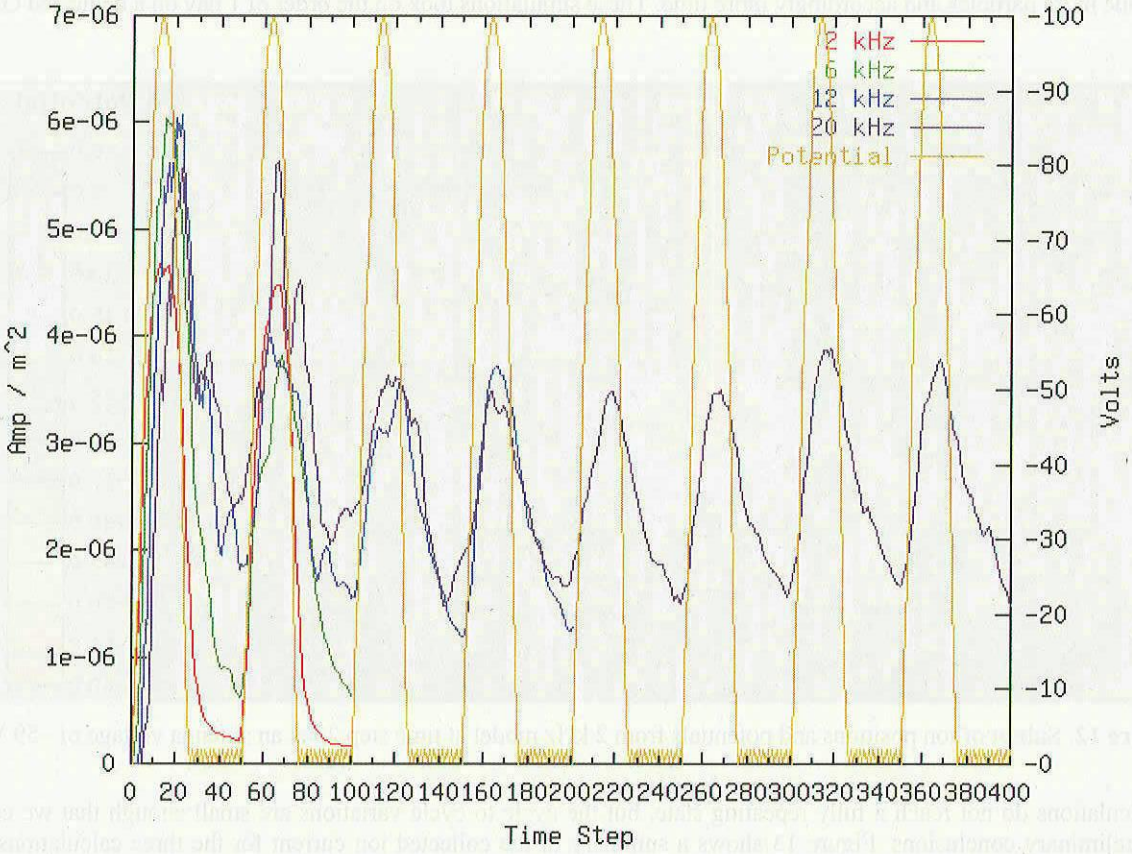

Figure 14. Current waveform results for Hybrid PIC antenna calculation in a thermal plasma at 2, 6, 12, and 20 kHz.

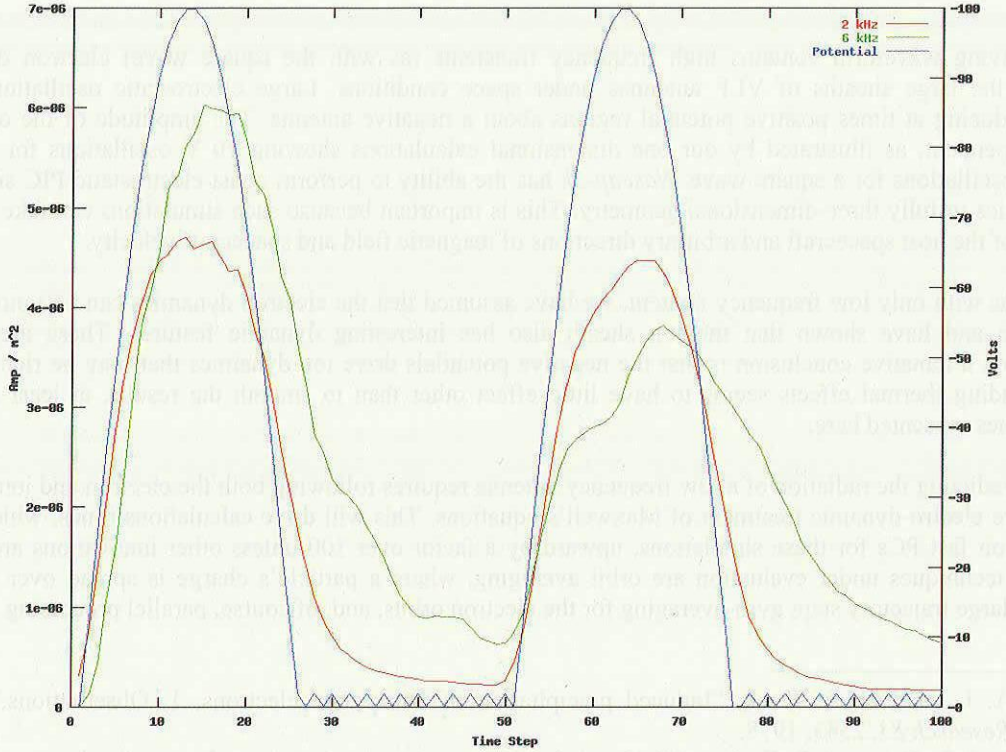

Figure 15. Current waveforms for the 2 kHz and 6 kHz cases at finite temperature.

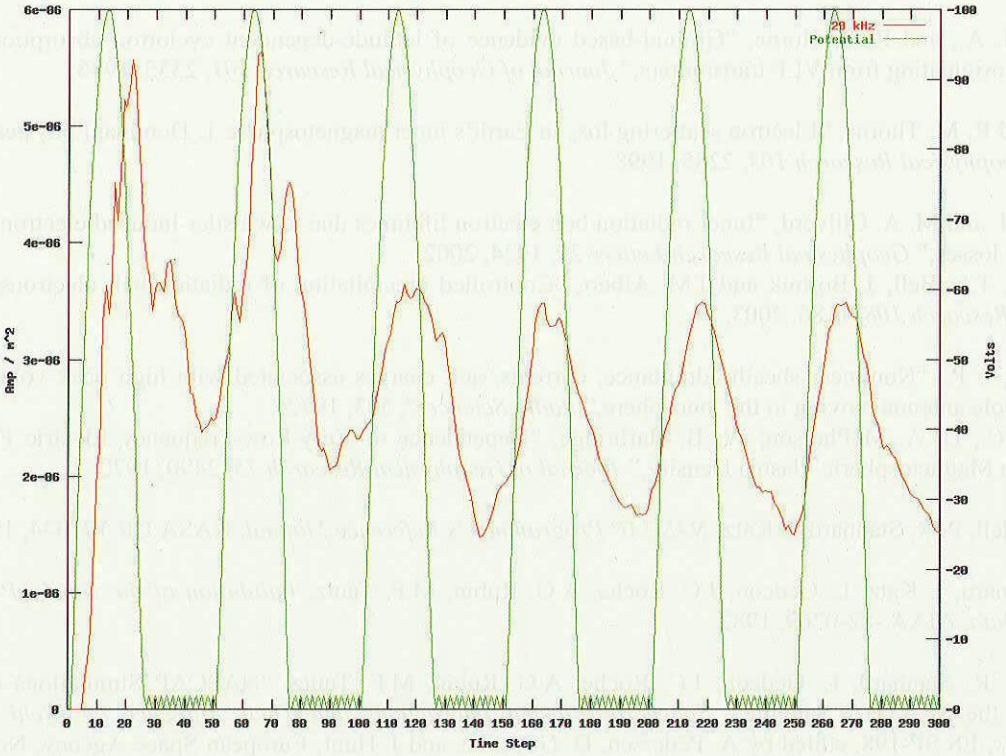

Figure 16. Current waveforms for the 20 kHz case at finite temperature.

Conclusions

When the driving waveform contains high frequency transients (as with the square wave) electron dynamics are important in the large sheaths of VLF antennas under space conditions. Large electrostatic oscillations are to be expected, producing at times positive potential regions about a negative antenna. The amplitude of the oscillations is waveform dependent, as illustrated by our one dimensional calculations showing 10 V oscillations for a sine wave versus 70 V oscillations for a square wave. *Nascap-2k* has the ability to perform quasi-electrostatic PIC simulations of sheath dynamics in fully three-dimensional geometry. This is important because such simulations can take into account the presence of the host spacecraft and arbitrary directions of magnetic field and spacecraft velocity.

For waveforms with only low frequency content, we have assumed that the electron dynamics can be ignored as a first approximation and have shown that the ion sheath also has interesting dynamic features. These are preliminary calculations but a tentative conclusion is that the negative potentials drive ion dynamics that may be rich in harmonic content. Including thermal effects seems to have little effect other than to smooth the results, at least for the short simulation times presented here.

Ultimately, predicting the radiation of a low frequency antenna requires following both the electron and ion dynamics as well as a more electro-dynamic treatment of Maxwell's equations. This will drive calculations times, which have been 10s of hours on fast PCs for these simulations, upward by a factor over 100 unless other innovations are introduced. Some of the techniques under evaluation are orbit averaging, where a particle's charge is spread over the full path covered by a large trajectory step; gyro-averaging for the electron orbits, and, of course, parallel processing.

---

[1] Vampola, A. L., and G. A. Kuck, "Induced precipitation of inner zone electrons, 1, Observations," *Journal of Geophysical Research 83*, 2543, 1978.
[2] Imhof, W. L., E. E. Gaines, J. B. Reagan, "Evidence for the resonance precipitation of energetic electrons from the slot region of the radiation belts," *Journal of Geophysical Research 79*, 3141, 1974.

[3] Inan, U. S., H. C. Chang, R. A Helliwell, "Electron Precipitation Zones Around Major Ground-Based VLF Signal Sources," *Journal of Geophysical Research 89*, 2891, 1984.

[4] Clilverd, M. A., and R. B. Horne, "Ground-based evidence of latitude-dependent cyclotron absorption of whistler mode signals originating from VLF transmitters," *Journal of Geophysical Research 101,* 2355, 1996.

[5] Abel, B. and R. M. Thorne, "Electron scattering loss in Earth's inner magnetosphere 1. Dominant physical processes," *Journal of Geophysical Research 103,* 2285, 1998.

[6] Rodger, C. J. and M. A. Clilverd, "Inner radiation belt electron lifetimes due to whistler-induced electron precipitation (WEP) driver losses," *Geophysical Research Letters 29*, 1924, 2002.
[7] Inan, U. S., T.F. Bell, J. Bortnik and J.M. Albert, "Controlled precipitation of radiation belt electrons," *Journal of Geophysical Research 108,* 1186, 2003.

[8] Shkarofsky, I. P., "Nonlinear sheath admittance, currents, and charges associated with high peak voltae drive on a VLF/ELF dipole antenna moving in the ionosphere," *Radio Science 7*, 503, 1972.
[9] Koons, H. C., D. A. McPherson, W. B. Harbridge, "Dependence of Very-Low-Frequency Electric Field Antenna Impedance on Magnetospheric Plasma Density," *Journal of Geophysical Research 75,* 2490, 1970.

[10] M. J. Mandell, P. R. Stannard, I. Katz, *NASCAP Programmer's Reference Manual,* NASA CR 191044, 1993.

[11] P. R. Stannard, I. Katz, L. Gedeon, J.C. Roche, A.G. Rubin, M.F. Tautz, *Validation of the NASCAP Model using Spaceflight Data*, AIAA -82-0269, 1982.

[12] I. Katz, P. R. Stannard, L. Gedeon, J.C. Roche, A.G. Rubin, M.F. Tautz, "NASCAP Simulations of Spacecraft Charging of the SCATHA Satellite," *Spacecraft/Plasma Interactions and Their Influence on Field and Particle Measurements*, ES SP-198, edited by A. Pedersen, D. Guyenne, and J. Hunt, European Space Agency, Noordwijk, The Netherlands, p. 190, 1983.

[13] M.J. Mandell and V.A. Davis, *User's Guide to NASCAP/LEO,* SCUBED report number SSS-R-85-730-R2. 1990.

[14] M.J. Mandell, and I. Katz, "High Voltage Plasma Interactions Calculations Using NASCAP/LEO," AIAA Paper AIAA-90-0725, 1990.

[15] J.R. Lilley, Jr., D.L. Cooke, G.A. Jongeward, I. Katz, *POLAR User's Manual*, GL-TR-89-0307, Oct. 1989.

[16] I. Katz, G.A. Jongeward, V.A. Davis, M.J. Mandell, R.A. Kuharski, J.R. Lilley, Jr., W.J. Raitt, D.L. Cooke, R.B. Torbert, G. Larson, and D. Rau, Structure of the Bipolar Plasma Sheath Generated by SPEAR I, *J. Geophysical Research, 94*, A2, p. 1450, 1989.

[17] M.J. Mandell, G.A. Jongeward, D.L. Cooke, W.J. Raitt, "SPEAR 3 flight analysis: Grounding by neutral gas release and magnetic field effects on current distribution," *J. Geophys. Res. 101*, A1, p. 439, 1998.

[18] V.A. Davis, M.J. Mandell, D.L. Cooke, and C.L. Enloe, High-voltage interactions in plasma wakes: Simulation and flight measurements from the Charge Hazards and Wake Studies (CHAWS) experiment, *J. Geophys. Res., 104,* A6, p. 12445, 1999.

[20] Davis, V.A., M.J. Mandell, D.L. Cooke and C.L. Enloe, "High-voltage interactions in plasma wakes: Simulation and flight measurements from the Charge Hazards and Wake Studies (CHAWS) experiment," *Journal of Geophysical Research 104*, No. A6, 12,445-12459, June 1999.